



Numerical modelling of CO₂ migration in heterogeneous sediments and leakage scenario for STEMM-CCS field experiments

Umer Saleem^a, Marius Dewar^{a,b}, Tariq Nawaz Chaudhary^a, Mehroz Sana^a, Anna Lichtschlag^d, Guttorm Alendal^c, Baixin Chen^{a,*}

^a Institute of Mechanical, Process and Energy Engineering, Heriot-Watt University, Edinburgh, EH14 4AS, UK

^b Plymouth Marine Laboratory, Prospect Place, Plymouth, PL1 3DH, UK

^c Department of Mathematics, University of Bergen, Bergen, Norway

^d National Oceanography Centre, Southampton, UK

ARTICLE INFO

Keywords:

STEMM-CCS, CO₂ injection
Two-phase flow in porous media
Porosity and grain size distribution
Gas migration
Darcy resistance
Carbon Capture and storage
CO₂ Leakage
Pipe flow
CO₂ dissolution

ABSTRACT

The dynamics and plume development of injected CO₂ dispersion and dissolution through sediments into water column, at the STEMM-CCS field experiment conducted in Goldeneye, are simulated and predicted by a newly developed two-phase flow model based on Navier-Stokes-Darcy equations. In the experiment, CO₂ gas was released into shallow marine sediment 3.0 m below the seafloor at 120 m water depth in the North Sea.

The pre-experimental survey data of porosity, grain size distributions, and brine concentration are used to reconstruct the model sediments. The gas CO₂ is then injected into the sediments at a rate of 5.7 kg/day to 143 kg/day. The model is validated by diagnostic simulations to compare with field observation data of CO₂ eruption time, changes in pH in sediments, and the gas leakage rates. Then the dynamics of the CO₂ plume development in the sediments are investigated by model simulations, including the leakage pathways, the fluids interactions among CO₂/brine/sediments, and CO₂ dissolution, in order to comprehend the mechanisms of CO₂ leakage through sediments. It is shown from model simulations that the CO₂ plume develops horizontally in the sediments at a rate of 0.375 m/day, CO₂ dissolution in the sediments is at an overall average rate of 0.03 g/sec with some peaks of 0.45 g/sec, 0.15 g/sec, and 0.3 g/sec, respectively, following the increase in injection rates, when some fresh brine provided. These, therefore, lead to a ratio of 0.90~0.93 of CO₂ leakage rate to injection rate.

1. Introduction

Carbon capture and storage (CCS) is a vital solution to mitigate the climate change and/or ocean acidification accompanying anthropogenic carbon dioxide (CO₂) level increasing by more than 25% since 1959 (NOAA 2020). The carbon emission has resulted in global warming of 1.5°C above pre-industrial levels and affected natural habitats on/off shore (IPCC 2018). CCS offers a solution of the disposal of carbon dioxide (CO₂) in the overburden sub-seabed reservoirs/geological structures instead of emitting the gas into the atmosphere to meet the 'target' set by the Kyoto Protocol (Freund and Ormerod, 1997; Han et al., 2012).

The geological reservoirs can be chosen for long term storage of CO₂ in well-designed storage sites (Oleynik et al., 2020). The utmost important concern about implementing CCS, especially for CO₂ under seabed reservoir storage, is the leakage risk of the sequestered CO₂ to the ocean due to its environmental physicochemical impacts (Feely

et al., 2016). The impacts include the local acidification at the CO₂ leakage site (Sokolowski et al., 2020; Yang et al., 2019) and the effects on marine life and ecosystem (Amaro et al., 2018; Jones et al., 2015; Molari et al., 2019). Therefore, it is necessary to understand the leakage mechanisms, then to estimate or predict the potential of the leakage to reduce the associated risks.

For under-seabed storage, studies have been made from Lab experiments (Li et al., 2020; Uemura et al., 2011), the natural CO₂ migration through geof ormations into the ocean, to the designed filed experiments, in collaboration with the studies of CO₂ ocean storage (Dewar et al., 2013; Caudron et al., 2012; McGinnis et al., 2011; Esposito et al., 2006). It has been recognized that CO₂ leakage developments are at a range of spatial scales from pore (~mm) in the geof ormation, the bubble/droplet (~ cm) once leaked into ocean, then the regional (~ 10² km) to global in the ocean. Liquid and gas phase CO₂ plume developments in turbulent ocean has been observed from small scale field experiments

* Corresponding author.

E-mail address: b.chen@hw.ac.uk (B. Chen).

<https://doi.org/10.1016/j.ijggc.2021.103339>

Received 11 December 2020; Received in revised form 1 April 2021; Accepted 12 April 2021

Available online 29 April 2021

1750-5836/Crown Copyright © 2021 Published by Elsevier Ltd. All rights reserved.

(Kim et al., 2019; Rhino et al., 2016) and modeled by means of computational fluid dynamics (CFD) (Dewar et al., 2013; Drange et al., 1993) (Umer, add this paper to here, Sato, T.; Sato, K. Numerical prediction of the dilution process and its biological impact on CO₂ ocean sequestration. *J. Marine Sci. Technol.* 2002, 6, 169-180.) and a kind of integral plume models (Dissanayake et al., 2018). The data of changes in pH from these small-scale plume models has been successfully implemented, as the input parametric data for plume further movements, in the large-scale ocean models (Blackford et al., 2020) once CO₂ leaks from seabed. On the other hand, the CO₂ mitigation from storage reservoirs to sediments were widely investigated from the field observations (Furre et al., 2017), the Lab experimental studies (Rillard et al., 2015; Tongwa et al., 2013) and numerical simulations (Discacciati et al., 2002; Du et al., 2016; Cai et al., 2009; Chidyagwai and Rivière, 2010). However, leakage from sediments into the ocean turbulent bottom boundary layers (TBBL) has been less focused, which, however, is one of the key processes for assessments of the biological impacts of leaked CO₂ on the ocean, as a rich population of marine organisms resides within both the ocean TBBL and shallow sediments. It is the dynamics of CO₂ migration and dissolution crossing the interface between shallow sediments and oceanic TBBL that dominate the leakage sources to the plumes evaluations in the ocean (Caudron et al., 2012).

In order to ensure the effective environmental monitoring of offshore CCS storage sites, the Strategies for Environmental Monitoring of Marine Carbon Capture and Storage (STEMM-CCS) project was launched in 2016 (Blackford et al., 2018), following previous field experiments QICS (Taylor et al., 2015) and ECO2 (Furre et al., 2017). STEMM-CCS is a scientific research project to simulate a sub-seafloor CO₂ leak under real-life conditions in the North Sea (Blackford et al., 2018). One of the primary objectives of the project is to produce experimental data for the development and calibration of numerical models to simulate the leakage dynamics of CO₂ out of the geoformations with the knowledge of dispersion time, pathways through faults and high permeable zones. In terms of marine physiochemical and biological impacts, for instance, the changes in pH due to leaked CO₂ is one of the most significant data for the assessment of leakage and model calibrations. Adequate knowledge of CO₂ dispersion through complex structure geoformation and dissolution characteristics of developed plume are mandatory and vital towards the development of the leakage prediction models. Supported by the project, a so-called Arbitrary Navier-Stokes-Darcy multi-fluid flow model (AnsdMF) has been developed for simulations of CO₂ transportations through the sediments with complex structures into the turbulent ocean.

In this study, the AnsdMF model is applied to simulate and predict the dynamic processes of initiations and developments of CO₂ and CO₂ solution plumes from injection ports through sediments to the ocean current in STEMM-CCS experiment. The numerical model settings, including the data collections, analysis, and reconstruction of sediments, are discussed in Section 2. The overall methodology of the numerical model including sub models of mass, momentum, and interfacial interactions among fluid-fluid-solid are explained in Section 3. The analysis and discussions on the model diagnostic simulation results are made in Section 4 with the CO₂ injection through pipe and leakage scenario results. Finally, the conclusions are drawn in Section 5.

2. Model sediment setup and data collection

The CO₂ release experiment of STEMM-CCS project was carried out in the vicinity of the Goldeneye platform located in a sandstone formation of Early Cretaceous near Scotland beneath Moray Firth (56-60N) (Dean and Tucker, 2017). In this project, gas CO₂ supplied from gas tanks was controllably released from 3m underneath the seabed (Flohr et al., 2020). Ships, remotely operated vehicles (ROVs), autonomous underwater vehicles (AUVs), the gas sampling system, and related equipment and sensors were employed to measure the changes in physicochemical properties in seawater and brine and monitor the

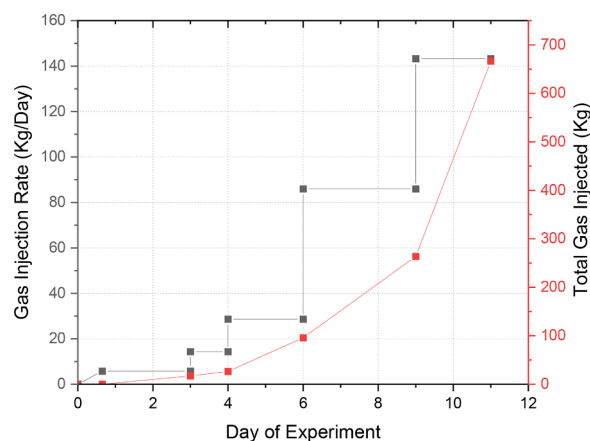


Fig. 1. Gas injection rate and total gas injected over the days from start injection collected from field experiment (Flohr et al., 2021).

leakages of CO₂. The gas release started on 11/05/2019 at 15:19hrs, which is set as the start of day 0 of the experiment (Flohr et al., 2021) in this study. The data of CO₂ injection rate and the total CO₂ injected, as shown in Fig. 1, are collected from field experiment as the input data of the modeling.

2.1. Porosity and grain size distribution

To set up the model sediments, AnsdMF requires data of particle size distributions and the porosity distributions of sediments. The data obtained from a project pre-survey were collected, which are those sampled in 18 boxes at different locations around CO₂ injection site down to 5.0 meters. The porosity data from core samples used in this study are plotted in Fig. 2, of which are the data from landers (POS527/si83 and gravity corer GC-06-Station-102), pockmarks (GC-01-Station-97 st.90/91 Obj 103), and well (GC-07-Station-103). The data shows that the average porosity is around 53% with +10% and -20% for the sediments deeper than 16 cm (Fig. 2 left), while, the decent distributions from surface to the depth of 16cm for shallow sediments (Fig. 2 right).

Another set of data requested from setting the model is the particle size distributions, which are taken from Particle size analysis (PSA) for various samples collected at different depths of sediments (Lichtschiag et al., 2021). A brief discussion on the characteristics of the particle distribution will help for model setting and for modelling the dynamic process of CO₂ gas penetration through sediments. From the data, shown in Fig. 3, it can be found that the deeper sediments, 3–4 m below the seabed (data of GC3 398-412cm), are mostly fine sand or laminated mud. The surface sediments down to about 0.5 m, however, are mostly particles of 60-100 μm with some smaller particles of less than 10 μm . In between those layers is a mixture of substances with varied grain sizes dominated within 8 to 100 μm . It must be noted that the very small particles within the sediments are more sensitive to additional disturbances, such as the penetration of CO₂ into the sediments, while the larger particles have a relatively larger inertia to withstand the disturbances and keep their original positions. This behavior of particles can be utilized for diagnostic setting of the model sediments for prediction of CO₂ dispersion with comparisons of observation data, such as the eruption time.

2.2. Reconstruction of model sediments by data

The heterogenous sediments are sediments with complex structure and various pore throat size distributions. The model requires the permeability distribution, intrinsic permeability at the first stage, to predict the resistant forces of fluids and porous solids. For the heterogenous sediment or rock, the throat size varies depending on the inter-

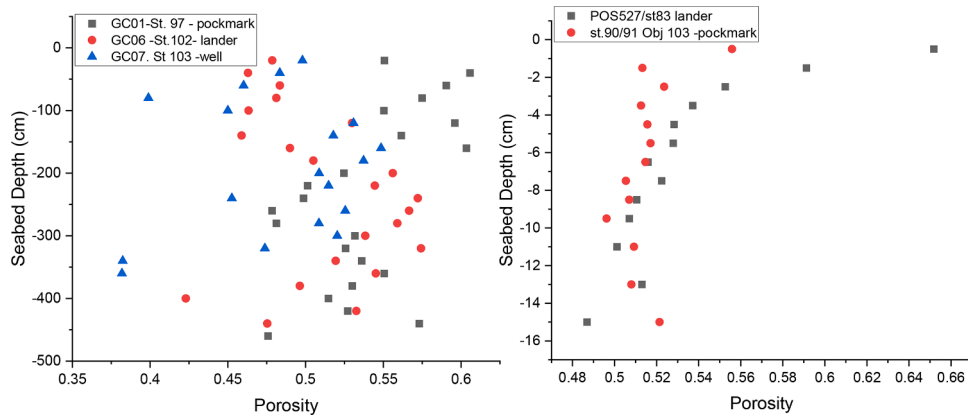


Fig. 2. Porosity distribution along the depth up to 500cm (left) and the shallow sediment (right) from various locations (Lichtschlag et al., 2021).

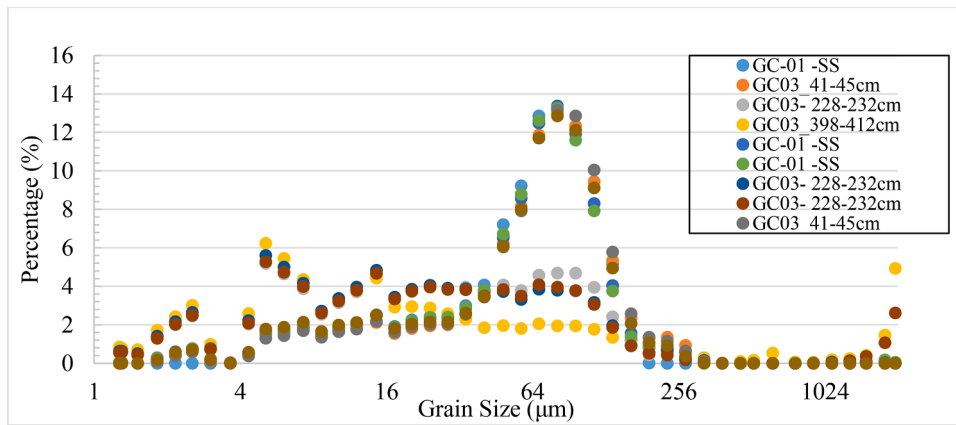


Fig. 3. Particle size density from various cores. GC01 to GC03 are the data from gravity cores followed by the depth in centimetre, while, the SS means the shallow sediments.

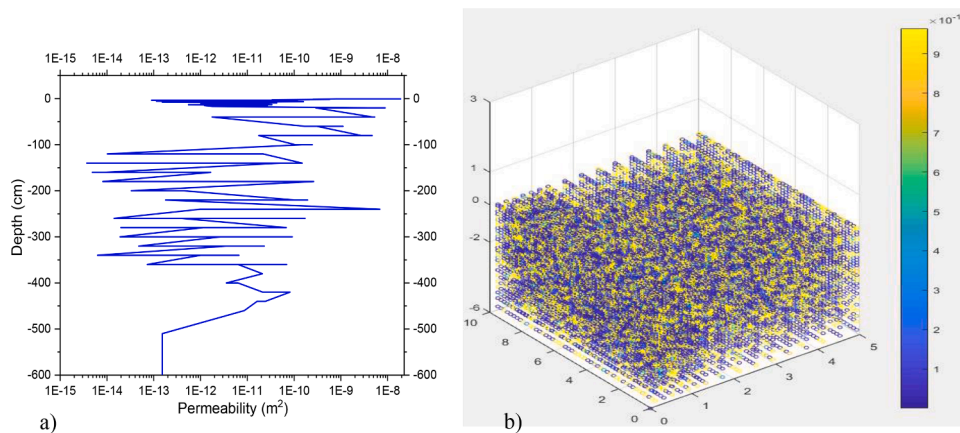


Fig. 4. (a) Horizontal Averaged Permeability distribution against depth calculated by Eq (1) using experimental data of particles size and porosity (shown in Fig. 2 and Fig 3, b) permeability distribution in the computational domain reconstructed.

connected pore structure and the pore size distribution, which is a function of porosity ϵ and particle size. Clay or poorly sorted silt shows lower permeability whereas coarse or well-sorted sediment, such as by shelly sands, shows high permeability (Phillips and Merritt, 2008). The correlations of permeability are mostly developed from the data of experiments and highly dependent on the structures of sediments. In this study, the Kozeny-Carman’s correlation (Henderson et al., 2010) for intrinsic permeability is applied for reconstructions of shallow sands

sediments,

$$K = \frac{d_p^2}{180} \frac{\epsilon^3}{(1 - \epsilon)^2} \tag{1}$$

where, K is intrinsic permeability (m^2) and d_p is the particles size (m). The data of porosity and particles size distributions from field observations, as shown in Figs. 2 & 3, are used to reconstruct the model sediments in terms of intrinsic permeability using Eq (1) and the

'topoSet' utility tool available on OpenFOAM (openfoam.org, (n.d.) 2020). The data with a range of the variation of both the porosity and particle size, at a given depth, are randomly taken to set the distributions of intrinsic permeability horizontally, meanwhile, the interpolations are made to set the data for the meshes in between the data available layers. The intrinsic permeabilities averaged at selected layers from reconstructed sediments can be found from Fig. 4 (a) and the reconstructed sediment demonstrated by intrinsic permeabilities for the computational domain of 10 m x 5 m (horizontal) x 7 m (vertical) for sediment is given in Fig. 4 (b). The permeability of the meshes between depth from 4.5 m to 7.0 m (no data available) is set by randomly selecting the data at layer 4.5 m. From such a reconstruction, it has been noticed that there are no specific structures, such as called as 'chimney' or 'fractures' or even the 'pockmarks' could be generated, which were identified from field observations at the leakage sites. In this study, such a complex structure sediment is generated by performing diagnostic simulations. The details can be found from Section 3.2.

The basic idea, based on general physics, is briefly described as follows. Fluids stored in the porosity of rocks produce pore pressure. Based on the magnitude, pore pressure can be normal/hydrostatic, sub-normal/sub-hydrostatic or abnormal/over pressured (Radwan et al., 2019). It depends on the sediments' strength that the formation or structure can bear the particular pressure before failing and developing to the fractures. When the pore pressure exceeds the overburden pressure due to CO₂ injection or flowing into, small diameter particles (mud or clay) may flow away to produce channels or fractures. The model sediments are reconstructed in such a way to simulate the effect of chimney, fractures, and pockmarks by using the data from observations (Section 2.1) and setting the cut-off grain sizes (the sizes of particles moveable) to create the chimney (or pipeline, fracture) in the sediments. The grain/particles smaller than the cut-off grain size are considered as the movable particles as CO₂ penetrates in. As shown from numerical experiments (Section 3.2), this cut-off grain size is diagnosed as 60 μm to represent the data of gas dispersion time of ~16 mins.

From the simulations of CO₂ dispersion and dissolution through the reconstructed sediments with grain size cut-off, it is also identified that the fine grains with size smaller than 60 μm could possibly be pushed up as like 'clay' to form the 'pockmarks' on the seafloor, providing the high permeability as observed from field survey. This means the gas could manage to create their own pathways; chimney, fracture channel or pipeline, by driving the fine size grains up from original place in the sediment. This can be demonstrated by the CO₂ plumes at the dispersion time (the time reaching to the seafloor), as described in Section 3.2.

3. Simulation model and governing equations

The dynamics of two-phase flows of leaked CO₂ flow through the sediments into the turbulent sea bottom boundary layers (BBL) are modeled by a set of Navier-Stokes-Darcy equations under assumptions of fluids and sediment are in a thermal equilibrium state with no thermal impacts considered, e.g., the dissolution heat, within model considered scales of 10 to 20 meters in this study. The model simulates the mass and momentum exchanges of fluids/phases in Eulerian scheme and couples the turbulent ocean flows with the flows in sediments. Due to the dynamics coupling of ocean current, the fluids flow in the sediments can be generated by the flows of BBL. The momentum interactions between phases/fluids are modeled individually by implementing the correlations from either the experimental data or theoretical analysis into the governing equations as source terms.

Considering the multiphase flows, the ensemble averaged continuity equations for phase φ can be written as

$$\frac{\partial \alpha_\varphi \varepsilon \rho_\varphi}{\partial t} + \frac{\partial}{\partial x_i} \left(\varepsilon \alpha_\varphi \rho_\varphi \bar{U}_{\varphi,i} \right) = \dot{S}_{m,\varphi} \quad (2)$$

where α_φ , ρ_φ and $\bar{U}_{\varphi,i}$ are the volume fraction, density, and the average

velocity of phase φ . ε represents the porosity of sediments and $\dot{S}_{m,\varphi}$ is a source term of the interphase mass transfer. Hence, in the BBL of ocean, ($\varepsilon \rightarrow 1$), Eq. (2) shrinks to a closing form of conditionally averaged continuity equation of phase φ as,

$$\frac{\partial \alpha_\varphi}{\partial t} + \nabla \cdot \left(\alpha_\varphi \bar{U}_{\varphi,i} \right) + \nabla \cdot \left(\alpha_\varphi (1 - \alpha_\varphi) \bar{U}_{r,i} \right) = \dot{S}_{\alpha,\varphi} \quad (3)$$

The last term on the left side of Eq. (3) is the term for restoring immiscibility condition of the two fluids with $\bar{U}_{r,i}$ the characteristic compression velocity of the interface sharpening can be predicted by the relative velocities between the fluids. Here in this paper, $\varphi = 1$ and $\varphi = 0$ represent the CO₂ and seawater, respectively.

Considering the interactions among phases/fluids and solid pore structure sediments, the ensemble averaged momentum equations for phase φ are given by:

$$\begin{aligned} \frac{\partial \varepsilon \alpha_\varphi \rho_\varphi \bar{U}_{\varphi,i}}{\partial t} + \frac{\partial}{\partial x_j} \left(\varepsilon \alpha_\varphi \rho_\varphi \bar{U}_{\varphi,i} \bar{U}_{\varphi,j} \right) + \frac{\partial}{\partial x_j} \left(\varepsilon \alpha_\varphi \rho_\varphi \bar{R}_{\varphi,i} \right) \\ = -\varepsilon \alpha_\varphi \nabla \bar{p}_\varphi + \nabla \cdot \left(\varepsilon \alpha_\varphi \bar{\tau}_\varphi \right) + \varepsilon \alpha_\varphi \rho_\varphi g + F_{b,\varphi} + \varepsilon M_\varphi - M_{\varphi,s} \end{aligned} \quad (4)$$

where, $\bar{R}_{i,j}$ is the combined Reynolds turbulent stress, \bar{p} the pressure, \bar{M}_φ the averaged inter-fluid phase momentum transfer term, $F_{b,\varphi}$ the body force, and $\bar{M}_{\varphi,s}$ the total resistance source term from sediments derived using Darcy-Forchheimer's law, of which should be modelled for the simulations.

The inter-fluid phase momentum transfer includes the instantaneous drag, lift, virtual mass and Basset forces, of which only the drag force (F_d) is considered in this study as it dominates,

$$M_\varphi = \alpha_\varphi F_d / V \quad (5)$$

where V is the volume of the dispersed phase element (DPE) and,

$$F_d = \frac{1}{2} \rho_\varphi A C_d \left| \bar{U}_r \right| \bar{U}_r \quad (6)$$

where A is the projected area of dispersed phase that is normal to relative velocity \bar{U}_r and C_d is drag coefficients of fluid φ to another. The C_d depends on the properties of DPE (as a rigid or spherical etc) and usually determined empirically from experiment data. In this study, C_d is estimated by (Gor et al., 2013),

$$C_d = \frac{24}{Re} (1 + 0.15 Re^{0.687}) \quad (7)$$

The force of buoyancy (the body force, $F_{b,\varphi}$) is implemented to the pressure gradient, as suggested by Rusche to get the pressure modified (Rusche, 2002), as such that the hydrostatic pressure is subtracted from the static pressure which is more convenient for treatments of the contact of each phase with wall.

In the sediments or porous zones, the macro-scale resistance forces for each phase φ as the fluid-solid interaction force can be predicted by (Darcy, 1856)

$$\bar{M}_{\varphi,s} = \left(\frac{\mu_\varphi}{K k_{r,\varphi}} \right) \bar{U}_\varphi \quad (8)$$

where μ is viscosity of fluids, the intrinsic permeability K (m²) has been set as discussed in Section 2, and $k_{r,\varphi}$ the relative permeability. The correlation of relative permeability proposed by Brooks and Corey (Brooks and A., 1964), which is an extended version of Corey's proposal (Corey, 1954), is applied in this study,

$$\begin{aligned} (S_e)^{\frac{2+3\lambda}{\lambda}} \varphi = 0 \\ k_{r,\varphi} = (1 - S_e)^2 \left(1 - S_e^{\frac{2+3\lambda}{\lambda}} \right) \varphi = 1 \end{aligned} \quad (9)$$

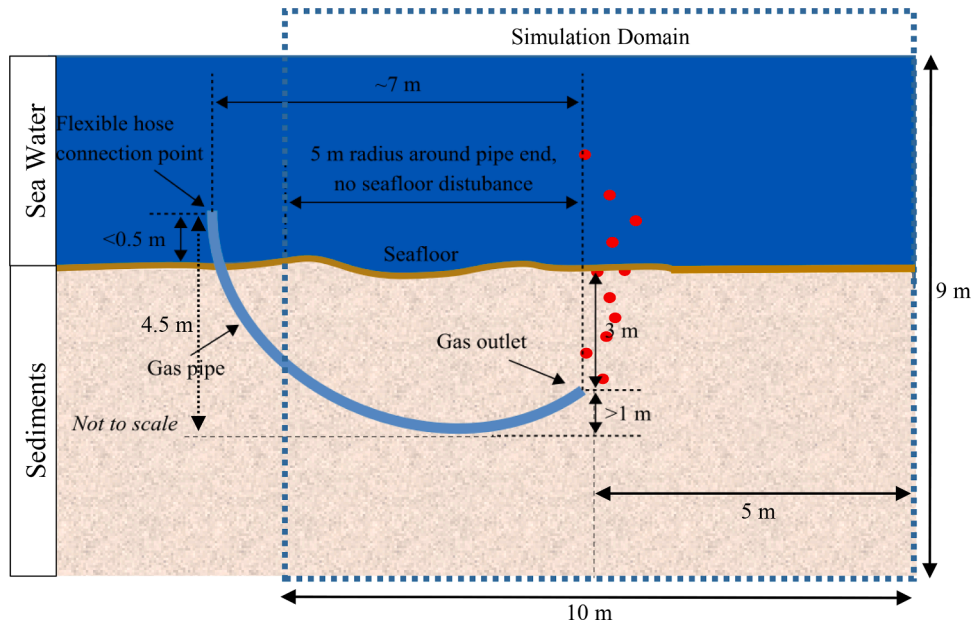


Fig. 5. The schematics of model simulation set up and computation domain for simulations of STEMM-CCS field experiment.

where, S_e is the effective saturation and defined as:

$$S_e = \frac{S_w - S_{wr}}{1 - S_{wr}} \quad (10)$$

with S_w as the wetting phase (brine) saturation and S_{wr} the residual saturation of the wetting phase (brine). λ is a parameter for distribution of pore sizes, which is set to $\lambda > 2$ for narrow distributions and $\lambda \leq 2$ for wide distributions (Brooks and A., 1964).

The mass conservation of each component in a considered element, can be derived as,

$$\frac{\partial \epsilon \alpha_\phi \rho_\phi Y_{\phi,k}}{\partial t} + \frac{\partial \epsilon \alpha_\phi \rho_\phi Y_{\phi,k} \bar{U}_{\phi,i}}{\partial x_j} - \frac{\partial \epsilon \alpha_\phi D_{\phi,k} \nabla Y_{\phi,k}}{\partial x_j} = \dot{S}_{\phi,k} \quad (11)$$

where Y_ϕ is the mass fraction of the species, $Sc_\phi = 0.7$ is the Schmidt number for prediction of effective diffusivity, and $\dot{S}_{\phi,k}$ denotes the mass transfer rate of species. In this study, only the CO_2 solution, $Y_{1,1}$ in brine and seawater is considered, for which, the $\dot{S}_{1,1}$ is the dissolution rate of CO_2 ,

$$\dot{S}_{m,\phi} = k_{\phi,k} A_{\phi,k} (C_s - C_o) \quad (12)$$

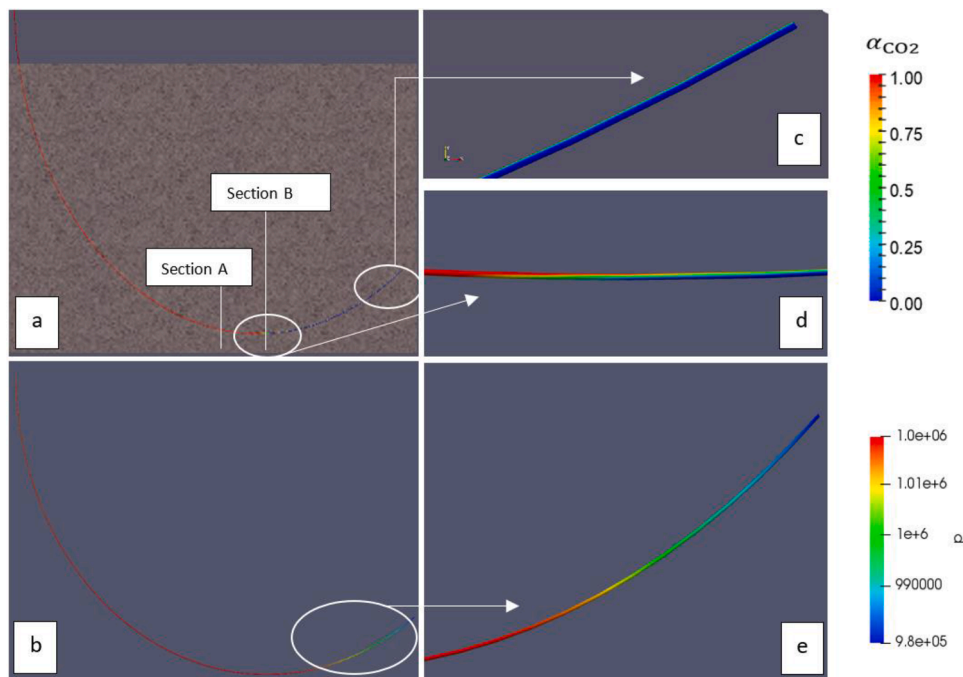


Fig. 6. Model simulation results: (a) CO_2 (Red) distribution in injection pipe at injection rate of 5.7 Kg/day into water (Blue) pre-loaded in the pipe; (b) Pressure distribution in the pipe; (c) volume fraction (α_{CO_2}) at the outlet shows CO_2 gas flows through only partial of the pipe section; (d) the CO_2 volume fraction around bottom curvature; and (e) Pressure distribution zoom-in the outlet section of the pipe.

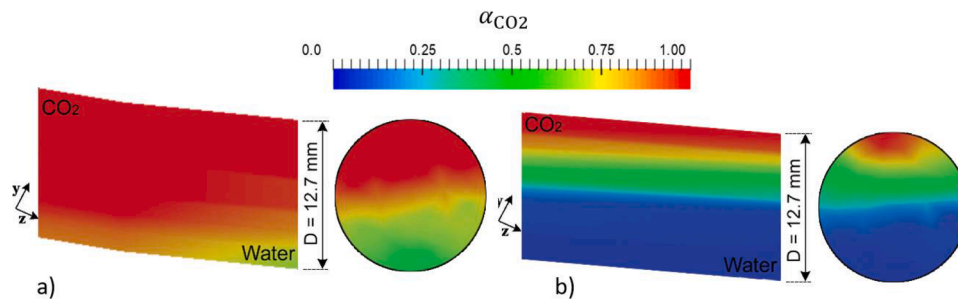


Fig. 7. Interactions of gas CO₂ ($\alpha_{CO_2} = 1$), CO₂ solution ($0 < \alpha_{CO_2} < 1$) and water ($\alpha_{CO_2} = 0$) in pipe at different sections indicated by CO₂ volume fraction, α_{CO_2} , from model simulations. a) a wave-like interface between CO₂ gas and CO₂ solution in the pipe at section A closing to the arc as indicated in Fig. 6 (a); b) the stratifications of gas CO₂, CO₂ solution and water in pipe closing to the centre of arc at section B shown in Fig. 6 (a).

where C_s is the solubility (in condensation) of CO₂ gas and C_o is the background concentration of dissolved CO₂ in brine/seawater; $k_{p,k}$ is the effective mass transfer coefficient and $A_{p,k}$ is the effective interfacial area between fluids, which are predicted by adjustments with the data from experiments (Jiang et al., 2017; Jiang et al., 2018).

3. Simulations of STEMM-CCS experiments

The AnsdMF model is applied to investigate the dynamics of plume developments of CO₂ gas and CO₂ solution in sediments for STEMM-CCS field experiments. The simulations consist of two parts, the pre-experiment simulations of CO₂ injection through injection pipe and the simulations of CO₂ dispersion through sediments with variant structures. The schematics of the computation domain and the related scales are shown in Fig. 5 for reference.

3.1. Pre-experiment simulation of CO₂ injection test

The flow of CO₂ through customized design of gas release system for STEMM-CCS experiment are simulated to predict the interactions of injected CO₂ gas with pre-loaded water in the U-shaped injection pipe, the dimensions and arrangement of the injection system can refer to Fig. 5. The intention of this simulation is to examine the possibility of back flow due to overburden sediments under a pressure of 12 bar and gas-liquid two-phase stratified flow behaviour at bottom curvature of pipe, which are the most concerns for the design of CO₂ injection system.

Results from model simulations identify the separations of injected CO₂ in the injection pipe at lower injection rate of 5.7 Kg/day, or at the initial stage of the injection. The dynamics of injected gas and water interactions at injection time of 3.5 minutes are discussed as follows. As for the downward part of the pipe (the left part of pipe shown in Fig. 6 (a)), the gas can manage to ‘push’ the water moving forward, while a separation of gas from water occurs closing to stationary point (Fig. 6, a and d).

This separation may be due to the interactions of inertia of water and the buoyancy of the gas (Duan et al., 2015; Chisholm, 1980). As such, in the upward part of the pipe, only partial of gas CO₂ can flow upwards and towards further (or inject) into the sediments, as shown in Fig. 6c & d.

A wave-like interface between CO₂ and water indicated by CO₂ volume fraction shows the instability of the flow by interactions of CO₂ and water (Fig. 7, a). The unstable stratification is identified at the interface between CO₂ solution and water, as shown at the arc of the pipe in Fig. 7, b).

Because of the separation, model simulations suggest that a higher injection pressure should be provided in order to keep the CO₂ gas injection rate, which is identified by the data from field experiment during the initial stage of injection (Flohr et al., 2020).

Table 1

results for various reconstructed model at grain size cut-off along with dissolution and plume diameter at the time of eruption/leakage.

Case	Cut-off Particle Size limit (D _p) (μm)	Eruption Time (T _E) (minutes)	CO ₂ Plume Size on the seafloor at Eruption (D _E) (m)	M _{dis} /M _{total}	Permeability (K) (m ²)
a	30	108	3.40	0.290	4.40952 × 10 ⁻¹⁴
b	36	72	3.21	0.289	9.83845 × 10 ⁻¹³
c	40	64	2.98	0.284	1.01031 × 10 ⁻¹³
d	45	42	2.66	0.277	1.14303 × 10 ⁻¹²
e	50	36	2.38	0.274	1.64711 × 10 ⁻¹²
f	52	33	2.31	0.270	2.67462 × 10 ⁻¹²
g	55	26	2.16	0.269	3.53409 × 10 ⁻¹²
h	60	16	2.08	0.267	8.32981 × 10 ⁻¹²

From the numerical diagnoses, the sediments with cut-off grain size of 60 μm is considered for the simulations of the STEMM-CCS field experiments to be discussed in the next section.

3.2. Investigation on the plume developments of CO₂ gas and CO₂ solution through sediments to water column

The model is then set for STEMM-CCS field experiments to diagnose the dynamics of CO₂ plume developments in sediments to ocean bottom boundary layer. The diagnostics are performed by injecting CO₂ into the reconstructed sediments with variants of cut-off grain size (refer to Section 2.2) in comparisons with field observation data, the time of CO₂ breakthrough. The three-dimensional 10 m x 9 m x 5 m computation domain is set with non-uniform mesh including a 6.0 m thick heterogeneous layer of sediments and a 3 m ocean on top of sediments as shown in Fig. 4 (b) and Fig. 5. The ocean current data from field observation is used to set the flows of water on the top of sediments.

The results of diagnostic simulations of the CO₂ plume developments through sediments reconstructed by setting the cut-off particles sizes from 30 μm to 60 μm are listed in Table 1 for cases I to VIII. An injection rate of 6 Kg/day CO₂ is used for the diagnostic discussions. The parameters for case checking are the CO₂ eruption time, the size of the CO₂ gas plume at ocean floor, the percentages of dissolved CO₂ in the sediments and those leaked to the ocean at the time of CO₂ eruption. The mesh independent test was performed to exclude the effects from grid-setting. The minimum mesh size is 0.5mm set at regions close to the injection port.

The first case is for the sediments using the original data shown in

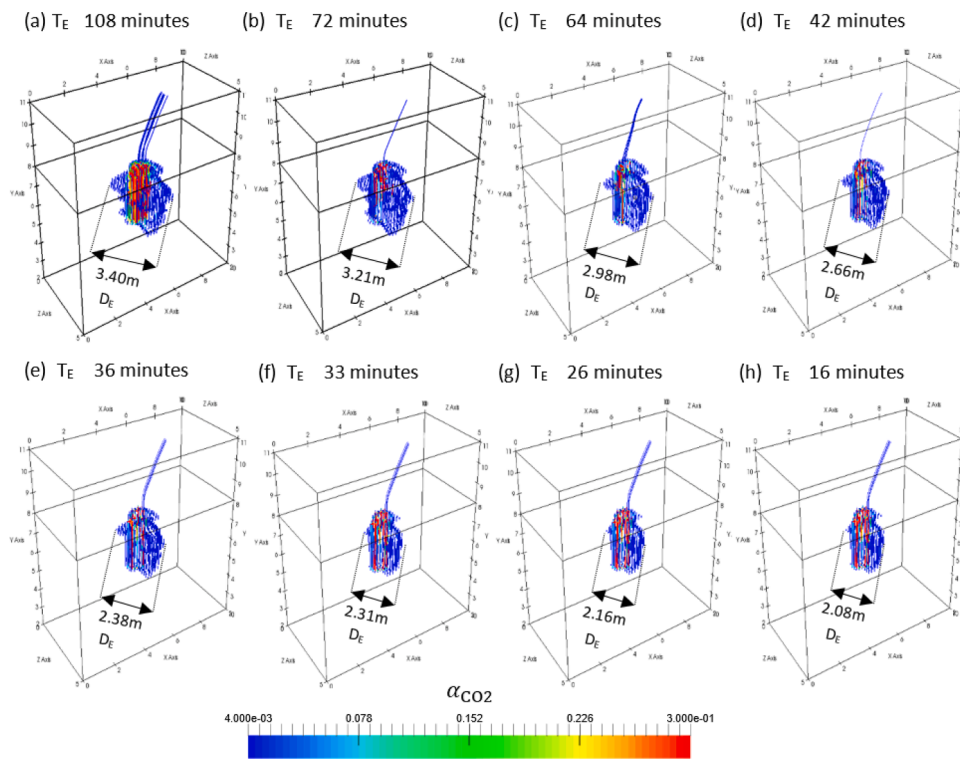


Fig. 8. The plumes of undissolved CO₂ in the sediments and water column at the time of breakthrough the sediments with the structure of cut-off grain sizes from 30 to 60 μm. The D_E is the maximum diameter of the plume in the sediment.

Fig. 3, for which the cut-off particle size is zero. This means that the original sediment filled with clay or sands is kept without fractures or pockmarks. The simulation results show that the injected CO₂ gas takes about 2.5 hours to flow through the sediment at a dispersion rate of 1.2 m/hr. Obviously, it is not the case of the field experiment, for which the pockmarks were observed and eruption time is about 16 min (Flohr et al., 2020).

When setting the cut-off particles, as listed in Table, I, the numerical experiment tests predicted that the larger the cut-off particle size set, the shorter the eruption time is, which decreases nonlinearly at a rate of 10 min per cut-off particle size. The same trend is witnessed for the area of CO₂ gas plume at sediment surface (D_E), which linearly decreases at a rate of 0.05 m per cut-off particle size. It seems not too sensitive to the dissolution of CO₂, which varies from 29% to 26% of the total injected CO₂ with time periods from 108 to 16 minutes. It is also noticed that the eruption time is approaching to the time observed from field experiment, when the cut-off size up to 60 μm. At the point of model diagnostics, this means that the sediments in the field experiments should form some pockmarks and create some fracture or ‘channels’ by CO₂ gas injection and dispersions to push and move the fine size grains/particles (< cut-off size) flowing upward.

This can be partially demonstrated by the plumes, as shown in Fig. 8 (note, the bottom part is sediments and top part is ocean), developed in variant of sediments at the eruption time. No significant differences are observed in general structure of the plumes from cut-off grain size < 40 μm, for which three horizontal branches are formed. The same for those of cut-off grain size at 40 μm to 50 μm, where only one horizontal branch forms. The CO₂ can manage to flow through the pathway with larger porosities, which are the left-side of the plumes for sediments of a-d, as shown in Fig. 8 with the red colour. When the cut-off grain size is set up at 50 μm to 60 μm, the plume could only develop within a certain horizontal region, meanwhile, two vertical flow pathways/channels (the red colour in Fig 8, f-h) are created to allow CO₂ gas to disperse fast toward to sediment surface without much dispersion horizontally. It is interesting to see a cap-like plume at the top layer of the sediments for all

of the cases, which are the result of ocean current and the relative larger porosities.

3.3. Simulations of CO₂ plume developments of STEMM-CCS field experiment

The developed model, AnsdMF, is applied to simulate the processes of CO₂ plume development in field experiment by injection of CO₂ at the rates recorded from experiments into the reconstructed sediments, which is diagnosed in last section with cut-off particle size of 60 μm. The CO₂ gas plume developed with time through sediments to water column is illustrated in Fig. 9 for the period of first 72 hours. It must be noticed that the dissolution of CO₂ in ocean water column is not modelled in the current version of AnsdMF, which means the plume in the water part are those of CO₂ gas bubbles with no dissolution, only for demonstration. However, this may have a neglectable effect on CO₂ gas developments inside the sediments, as there’s no significant variation in CO₂ solution plume developed from such a small leakage rate (Dewar et al., 2013), therefore, the ocean current dominates the flows of the seawater.

In addition to the vertical dispersion through the pathways that are created during the initial development period, it is interesting to see horizontal dispersions of CO₂ in the sediments eventually form a multilayer plume from the injection port. This structure of the plume is dominantly generated by the structure of sediments, the distribution of grain size and porosities. If the dynamic response of sediments on CO₂ dispersion could be modelled, this coupling model would provide the details of interactions among CO₂, brine, the sands of the sediments to predict the formations of chimney, fractures, and pockmarks and the movements of the leakage position on surface of the sediments.

The simulations predict that about 98% of injected CO₂ leaks into water column, while, about 1% dissolves into the brine and 1% remains as the gas in the sediment at release time up to 25 hrs. The details on CO₂ plume size in the sediments, the leakage rate, and the ratios of dissolved CO₂ and gas phase CO₂ in sediments are summarised and listed in Table 2 for th period of field release experiments to the day 11. The CO₂

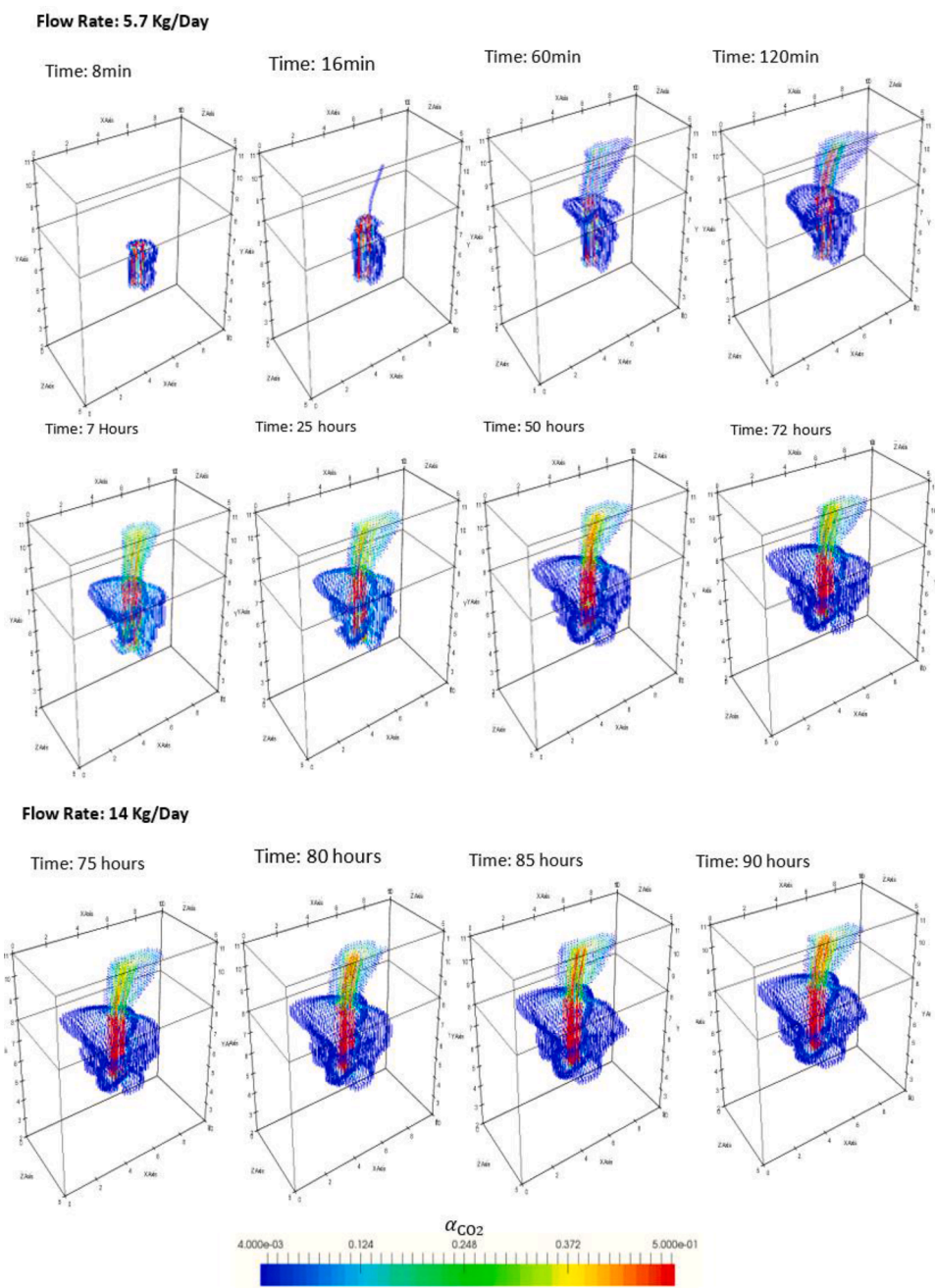


Fig. 9. The model results of developments of CO₂ gas plume in the field experiment up to time of 90 hours.

Table 2

Summaries of modelling simulation results on plume developments measured by maximum plume diameter, leakage rate, the ratios of dissolved CO₂ (M_{dis}), undissolved CO₂ (M_{undis}) and leaked CO₂ (M_{leaked}) to total injected CO₂ (M_{total}) at experimental date-time.

Time (Hours)	Day since Injection Started (Day +0)	Gas Injection Rate (Kg/Day)	Max. Plume Diameter inside Sediment (D_E) (m)	Leakage Rate (Kg/Day) (Avg.)	M_{dis}/M_{total}	M_{undis}/M_{total}	M_{Leaked}/M_{total}
14/05/2019 15:15	Day +3	5.7	3.51	5.11	0.038	0.024	0.938
15/05/2019 06:47	Day +4	14	4.72	10.10	0.010	0.008	0.982
17/05/2019 16:53	Day +6	29	4.92	24.37	0.005	0.006	0.989
19/05/2019 15:49	Day +8	86	5.11	70.12	0.001	0.001	0.998
22/05/2019 11:15	Day +11	143	6.51	132.2	0.002	0.001	0.997

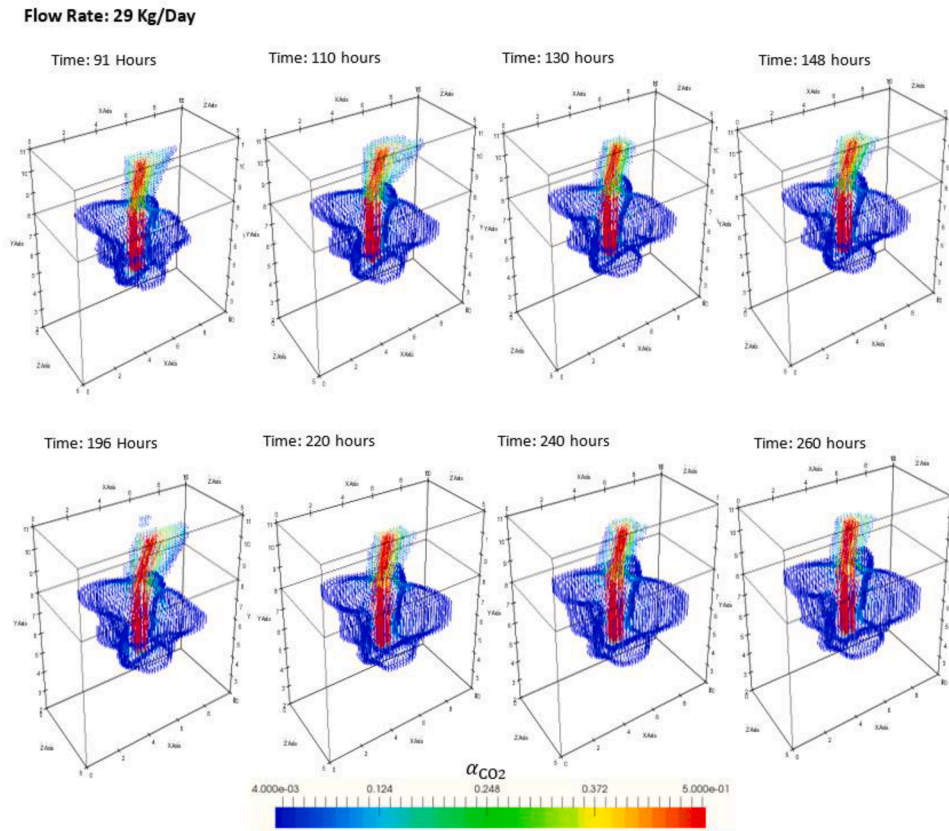


Fig. 10. The model results of developments of CO₂ gas plume in the field experiment up to time of 260 hours.

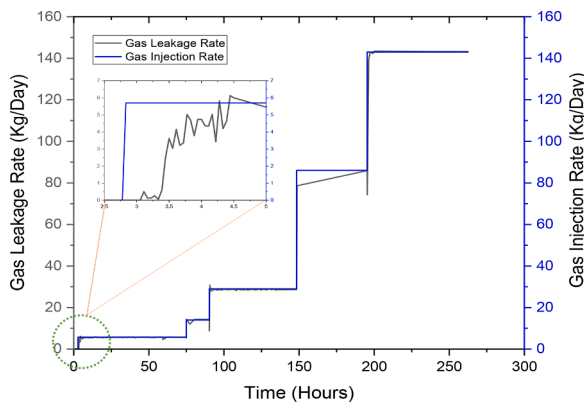


Fig. 11. CO₂ Gas leaking rate from sediments into water column and CO₂ injection rate. The sub-Fig show the details withing first 5 days.

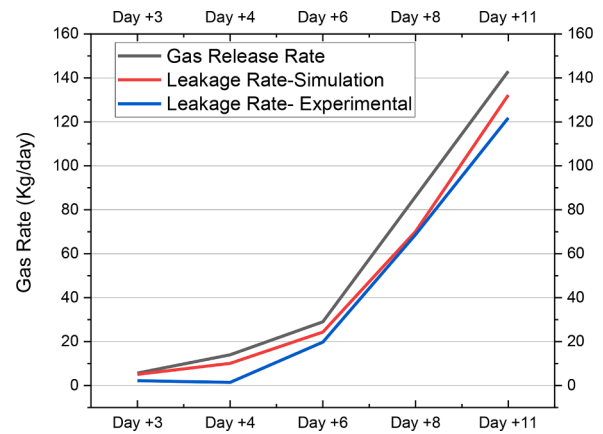


Fig. 12. Gas leakage rate comparison with experimental results.

Table 3
Leakage rate data from experiment and simulation.

Injection rate (kg/day)	Leakage rate (Experimental) (kg/day) ±14%	Leakage rate (Simulation) (kg/day)
5.7	2.21	5.11
14.3	1.44*	10.10
28.5	19.8	24.37
85.5	68.7	70.12
143	121.8	132.2

*: The 1.44 kg/day leakage rate at 14.3 kg/day is the weakest observation (Koopmans et al., 2021).

gas plume developments are shown in Fig. 9 and Fig. 10. Within the initial period, the CO₂ plume developments, measured by horizontal dispersion, at a rate of 3.75m/day. The percentage of CO₂ dissolution decreases from 3.8% to 0.2% as there is a lack of the fresh brine entering into the plume.

3.3.1. Discussions on CO₂ leakages

To further check the leakage rate, one of the key parameters for the oceanic impacts, the data up to the day 11 of injection from simulations is plotted in Fig. 11 together with CO₂ injection rate. The leakage rates at initial periods of 5 hours are given by the inside figure, which shows that the average leakage rate is about 3.0 kg/day. For comparisons, the observation data and modelling results on leakage rate associating with the injection rate are listed in Table 3 and shown in Fig. 12.

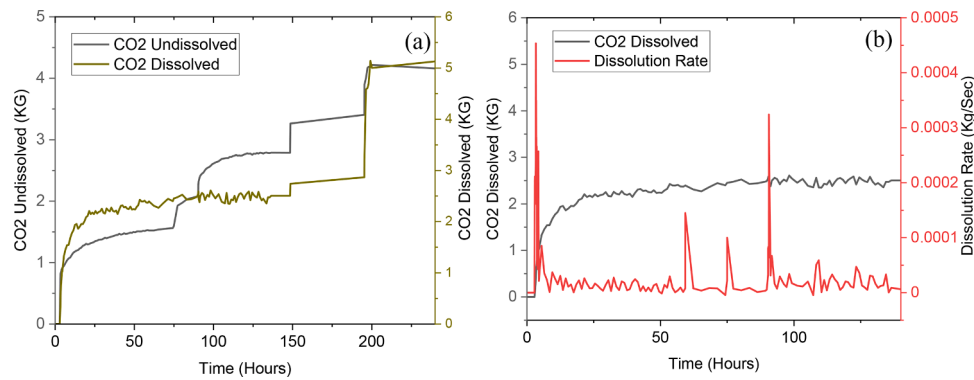


Fig. 13. (a) Total dissolved/undissolved CO₂ in the sediments up to 11 days of CO₂ injection (b) Results showing the total amount of gas dissolved in sediments and dissolution rate.

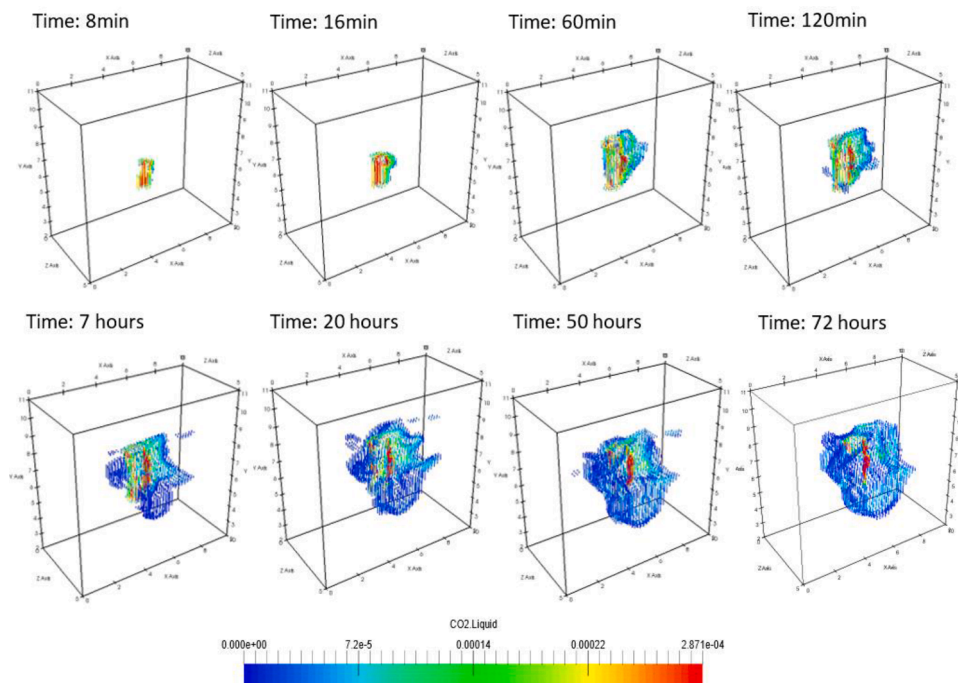


Fig. 14. Time evolutions of dissolved CO₂ plume from initiation to the injection day 3. The plume is demonstrated by CO₂ concentration in CO₂ solution.

During the release experiment, the CO₂ leakage rate was observed and determined from the eddy pH sensor and the complete procedure of leakage observation is introduced in (Koopmans et al., 2021). According to the discussions (Koopmans et al., 2021), an overall CO₂ leakage of 83% ± 14% was estimated under all gas release rates except one of 14.3 kg/day. The details on the field observations on CO₂ leakage rate can be found from publications (Koopmans et al., 2021; Schaap, 2021).

The experimental observation data show that the gas leakage initiated from ~2.21 kg/day to ~121.8 kg/day at a gas release rate from 5.7 kg/day to 143 kg/day, while, the results from simulations are 5.11 kg/day to 132.2 kg/day. As shown in Fig. 12, in general, it can be seen that the model works well in the overall period of injection for the predictions of leakage rates. It has to be noted that it is difficult at the moment to analyze or identify what may result in the differences between model results and observations as both have some uncertainties, e.g., the insufficient in dissolution rate modelling in the modelling side; the possibility of some undetectable or undetected measurements in the field experiments. If the uncertainties from modelling and observations were considered, the results obtained from model seem acceptable for impact/risk estimation, at least the results from observation and

modelling are at the same order of magnitude, especially those of 70.12 kg/day and 68.7kg/day from modelling and observation at the injection rate of 85.5 kg/day.

From modelling simulations, it is identified that initially, the lower CO₂ leakage rate is due to high dissolution rate with sufficient fresh brine for dissolution of CO₂ as the plume develops. The leakage rate increases to 10.10 kg/day due to slow horizontal dispersion of injected CO₂ and the straightforward movement through the pathway that was created from plume initiation, refer to Fig. 9 after the 75 hours of injection. This mechanism also can explain the larger leakage rate at day 11, which is 121.8 kg/day from observation (Koopmans et al., 2021) and 143 kg/day from simulation.

These results can be improved by increasing the porosity and grain size resolution. In this study, 2.0 cm resolution for porosity and grain sample is used. The increase in number of cores sampled may lead to more accurate sediment structure that can include the precise fracture openings directions, thicknesses, and locations.

3.3.2. Dissolution of CO₂ in pore-water

In this section, analysis is focused on CO₂ dissolution in sediment

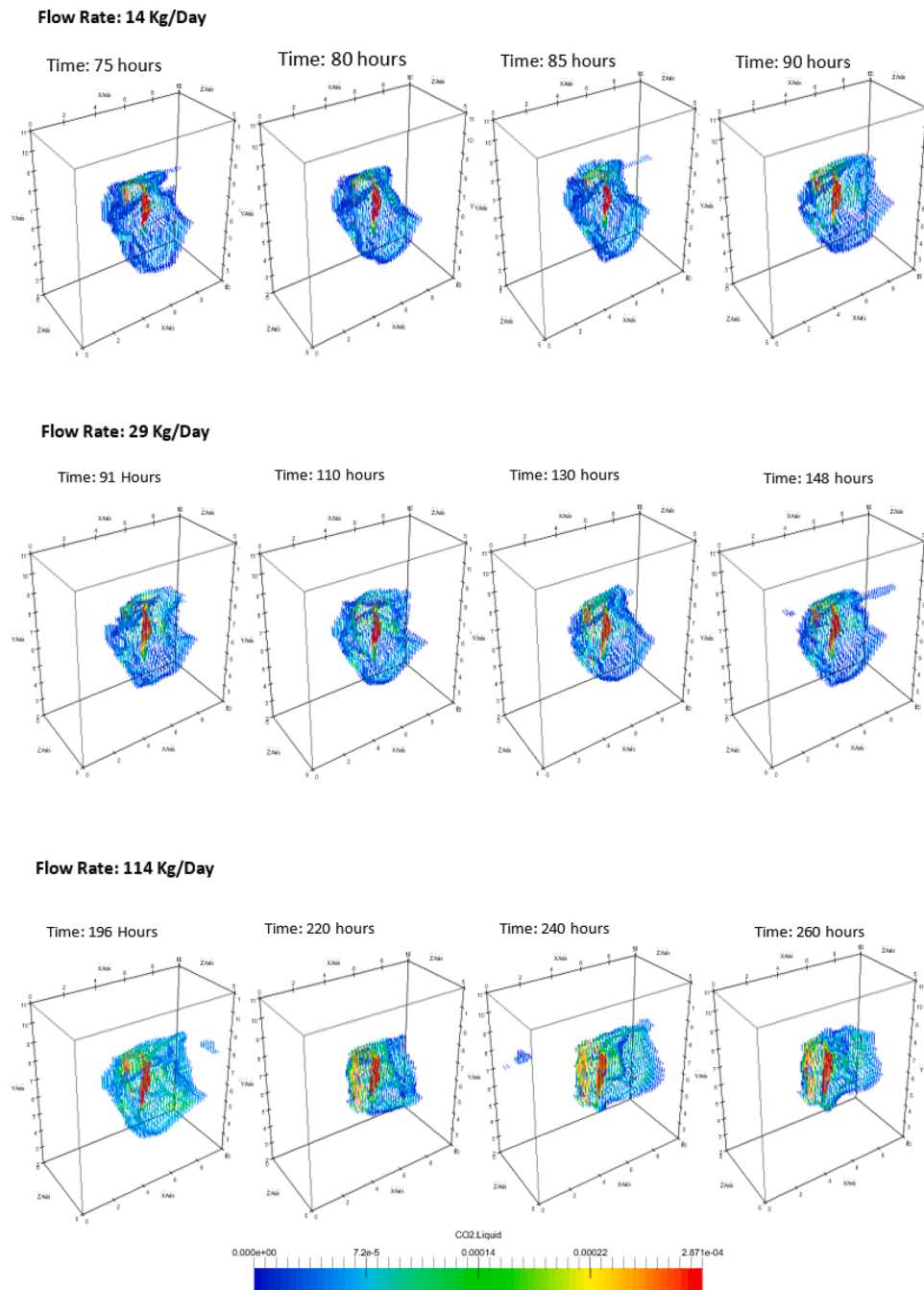


Fig. 15. The model results of developments of CO₂ solution plume in the field experiment from day 3 up to day 11. The plume is demonstrated by CO₂ concentration in solution.

from modelling simulations. The data collected from simulations is the total dissolved CO₂ and remained gas CO₂ in sediment, which are plotted in Fig. 13 (a). In order to reveal variations of dissolution with CO₂ injection, the rate of CO₂ dissolution is examined and the data are given in Fig. 13 (b). All of the data are collected from plumes of CO₂ solutions, which are shown in Fig. 14 to day 6 and in Fig. 15 for the following days to day 11. From Fig. 13, it can be seen that, as mentioned in the previous section, the injected CO₂ could find unsaturated brine to dissolve during the early period of plume initiations under the lower injections rate. These two factors, lower injection rate and the horizontal dispersions at a rate of 1.17 m/day, refer to the Table 2, leads the maximum dissolution rate, see the first peak in Fig. 13 (b), and amount of dissolved CO₂ is relatively larger than those of gas CO₂.

Due to the increases in injection rate to 14kg/day at 75 hrs and 29kg/

day at 90 hrs after injection, it turns more gas CO₂ in the sediment than those of dissolved. The increase in injection rate also leads to an increase in dissolution rate, the two peaks shown in Fig. 13 b, at associated times. However, the limitation in the horizontal developments of the plume makes it unable to keep the large dissolution rate, actually, as shown in Fig. 13 b) the average dissolution rate is about 3.0kg/day, which is much smaller than the injection rates. The peaks in dissolution rate are all at the time following the increase in injection rate, for which, as discussed previously, can be explained by the fact that an increase in injection rate leads to the horizontal expansion in CO₂ plume to provide some fresh brine to dissolve CO₂. Once the plume develops to a steady state after each injection increase, the dissolution is then back to the state governed by the horizontal dispersions of gas CO₂ and a general dissolution rate, as shown in Fig. 13 (b).

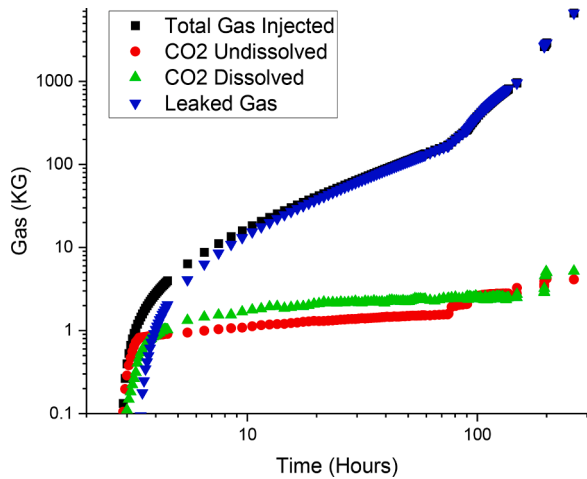


Fig. 16. The modelled distribution of injected CO₂, dissolved and undissolved CO₂ in sediments, and CO₂ leaked to water column.

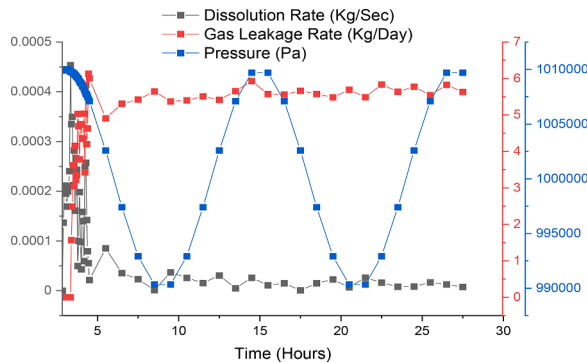


Fig. 17. Effect of tide (pressure) on dissolution rate and leakage rate.

The vertical transportation of CO₂ solution is much slower than that of CO₂ gas driven by buoyancy in addition to the injection pressure. This can be seen from CO₂ solution plume development, shown in Figs. 14 and 15. At the centre of the plume, the CO₂ solution reaches to the saturation state (red colour) quickly and develops into two branches. The horizontal movement of the plume may be driven by the in-sediment current developed by the ocean current towards to the right side of the computation domain. An obvious sinking of CO₂ solution can be identified by the downward plume penetration below the injection port. It must be noticed that the sink of CO₂ solution can be made by both the negative buoyancy due to the increase in density and the CO₂ injection, which creates a flow in all directions. The flow of brine and CO₂ solution should be generally induced by CO₂ injection in the sediments close to the injection point.

The distributions of CO₂ as the gas phase and solution in sediment and those leaked into ocean are examined from modelling simulations, and the results are given in Fig. 16. It is identified again that the CO₂ stored in sediment as solution and the gas CO₂ that stayed temporarily in sediment are of the same order of magnitude, say, 1.5 – 3.0 kg by the injection day 11. Meanwhile, those of CO₂ in the solution are mostly dissolved within the first day when the plumes are initiated (or initially developed) by dispersion through the pathways. As the results, about 90% of injected CO₂ should be leaked into the ocean water column from sediments in this field experiments, which is quite close to the data observed from experiment.

There are arguments on the effects of tide on CO₂ gas plume development in sediments and the leakages, which are checked from model simulations. In the simulations, a sinusoidal pressure wave was set on top of domain to simulate the physical behaviour of ocean tide. As

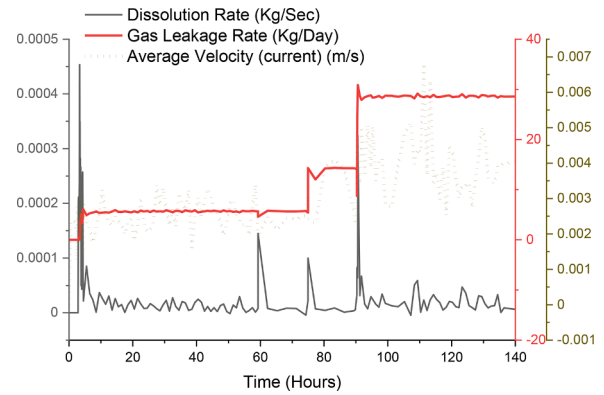


Fig. 18. Effect of ocean current on dissolution rate and leakage flux.

shown in Fig. 17 within one cycle of tide, it seems hard to identify the correlations between the tide waves (the changes in pressure) and CO₂ solution even though the leakage from this simulation study.

The effects of oceanic current on both the leakage and dissolution of CO₂ are preliminarily examined and the results are shown in Fig. 18. It looks that the fluctuations of dissolution rate somehow are coincided with the fluctuations of ocean current, however, as discussed in the previous sections, the dissolution rate is more dominantly affected by increase in injection rate.

4. Conclusion

The developed “arbitrary Navier-Stokes-Darcy multi-fluid flow model” (AnsdMF) is applied to simulate a controlled CO₂ release experiment in order to diagnosis the mechanisms of the evolution of gas in near subsurface migration pathways and breakthrough in the seawater. By simulating the CO₂-Water two phase flow in complex geofomations based with fractures, channels and pockmark physical data, it is identified that the model is capable of predicting the major mechanisms of CO₂ dispersion and dissolution in the sediments with complex structures of chimney/fracture/pockmarks.

By the reconstructed sediment, diagnosed by CO₂ eruption time, the model predicts for this experiment that most of the CO₂ stored in sediment, in solution phase, is dissolved within the first day of injection at a peak dissolution rate of 0.35 g/sec at the first hour of gas injection. The preliminary results of CO₂ leakage rates and total leaked CO₂ from model simulations are in general agreement with those of field observations. However, the uncertainties from both the developed model and observation measurements suggest that further investigations on the mechanism of CO₂ dissolution in sediments is needed. One of the key conclusions from modeling diagnostic studies is that the structure properties of sediment play a key role on CO₂ leakage, meanwhile, it is suggested that the CO₂ gas may be able to manage to create the pathways in the sediment by replacing or removing the mud or clay to create the fractures or ‘chimney’ to flow through. The dynamics and the mechanisms of these fractures or ‘chimney’ creation should be well investigated and a model should be developed.

Declaration of Competing Interest

The authors declare that they have no known competing financial interests or personal relationships that could have appeared to influence the work reported in this paper.

Acknowledgements

This research is supported by STEM-CCS project received funding from the European Union’s Horizon 2020 research and innovation programme under grant agreement No. 654462. In-kind contributions

from the University of Bergen are gratefully acknowledged. The authors also acknowledge the Research Council of Norway through the CLIMIT program funded project no 254711 (Baymode).

References

- NOAA. Atmospheric CO₂, Mauna Loa Observatory. <http://co2now.org/images/stories/data/co2-mlo-monthly-noaa-esrl.pdf> (accessed 03.06.20). 2020.
- IPCC, 2018. In: Masson-Delmotte, V., Zhai, P., Pörtner, H.-O., Roberts, D., Skea, J., Shukla, P.R., Pirani, A., Moufouma-Okia, W., Péan, C., Pidcock, R., Connors, S., Matthews, J.B.R., Chen, Y., Zhou, X., Gomis, M.I., Lonnoy, E., Maycock, T., Tignor, M., Waterfield, T. (Eds.), Summary for Policymakers. In: Global Warming of 1.5°C. An IPCC Special Report on the Impacts of Global Warming of 1.5°C Above Pre-Industrial Levels and Related Global Greenhouse Gas Emission Pathways, in the Context of Strengthening the Global Response to the Threat of Climate Change, Sustainable Development, and Efforts to Eradicate Poverty. World Meteorological Organization, Geneva, Switzerland, p. 32.
- Freund, P., Ormerod, W.G., 1997. Progress toward storage of carbon dioxide. *Energy Convers. Manage.* 38, S199–S204.
- Han, J.-H., Ryu, J.-H., Lee, I.-B., 2012. A preliminary infrastructure design to use fossil fuels with carbon capture and storage and renewable energy systems. *Int. J. Hydrogen Energy* 37 (22), 17321–17335.
- Oleyunik, A., et al., 2020. Optimal sensors placement for detecting CO₂ discharges from unknown locations on the seafloor. *Int. J. Greenhouse Gas Control* 95, 102951.
- Feeley, R.A., et al., 2016. Chemical and biological impacts of ocean acidification along the west coast of North America. *Estuarine Coastal Shelf Sci.* 183, 260–270.
- Schaap, A., et al., 2021. Quantification of a subsea CO₂ release with lab-on-chip sensors measuring benthic gradients. *Int. J. Greenhouse Gas Control* (STEMM-CCS).
- Sokolowski, A., Brulińska, D., Sokolowska, E., 2020. Multimarker response of the ragworm *Hediste diversicolor* (Polychaeta) to seawater acidification derived from potential CO₂ leakage from the CCS sub-seabed storage site in the Baltic Sea. *J. Exp. Mar. Biol. Ecol.* 530–531, 151433.
- Yang, Y.-M., et al., 2019. Integration of wellbore pressure measurement and groundwater quality monitoring to enhance detectability of brine and CO₂ leakage. *Int. J. Greenhouse Gas Control* 85, 143–155.
- Amaro, T., et al., 2018. Effects of sub-seabed CO₂ leakage: Short- and medium-term responses of benthic macrofaunal assemblages. *Mar. Pollut. Bull.* 128, 519–526.
- Jones, D.G., et al., 2015. Developments since 2005 in understanding potential environmental impacts of CO₂ leakage from geological storage. *Int. J. Greenhouse Gas Control* 40, 350–377.
- Molari, M., et al., 2019. CO₂ leakage can cause loss of benthic biodiversity in submarine sands. *Mar. Environ. Res.* 144, 213–229.
- Li, C., et al., 2020. A new method to protect the cementing sealing integrity of carbon dioxide geological storage well: an experiment and mechanism study. *Eng. Fract. Mech.* 236, 107213.
- Uemura, S., et al., 2011. Experiment on liquid and supercritical CO₂ distribution using micro-focus X-ray CT for estimation of geological storage. *Energy Procedia* 4, 5102–5107.
- Dewar, M., et al., 2013. Small-scale modelling of the physiochemical impacts of CO₂ leaked from sub-seabed reservoirs or pipelines within the North Sea and surrounding waters. *Mar. Pollut. Bull.* 73 (2), 504–515.
- Caudron, C., Mazot, A., Bernard, A., 2012. Carbon dioxide dynamics in Kelud volcanic lake. *J. Geophys. Res.: Solid Earth* 117 (B5).
- McGinnis, D.F., et al., 2011. Discovery of a natural CO₂ seep in the German North Sea: implications for shallow dissolved gas and seep detection. *J. Geophys. Res.: Oceans* (C3), 116.
- Esposito, A., Giordano, G., Anzidei, M., 2006. The 2002–2003 submarine gas eruption at Panarea volcano (Aeolian Islands, Italy): volcanology of the seafloor and implications for the hazard scenario. *Mar. Geol.* 227 (1), 119–134.
- Kim, J., et al., 2019. CO₂ leakage detection in the near-surface above natural CO₂-rich water aquifer using soil gas monitoring. *Int. J. Greenhouse Gas Control* 88, 261–271.
- Rhino, K., et al., 2016. The demo-CO₂ project: monitoring and comparison of two shallow subsurface CO₂ leakage experiments with gas tracer associated in the carbonate vadose zone. *Int. J. Greenhouse Gas Control* 53, 207–221.
- Drange, H., Alendal, G., Haugan, P.M., 1993. A bottom gravity current model for CO₂-enriched seawater. *Energy Convers. Manage.* 34 (9), 1065–1072.
- Furre, A.-K., et al., 2017. 20 Years of monitoring CO₂-injection at Sleipner. *Energy Procedia* 114, 3916–3926.
- Rillard, J., et al., 2015. The DEMO-CO₂ project: a vadose zone CO₂ and tracer leakage field experiment. *Int. J. Greenhouse Gas Control* 39, 302–317.
- Tongwa, P., et al., 2013. Evaluation of potential fracture-sealing materials for remediating CO₂ leakage pathways during CO₂ sequestration. *Int. J. Greenhouse Gas Control* 18, 128–138.
- Discacciati, M., Miglio, E., Quarteroni, A., 2002. Mathematical and numerical models for coupling surface and groundwater flows. *Appl. Numer. Math.* 43 (1–2), 57–74.
- Du, G., Hou, Y., Zuo, L., 2016. Local and parallel finite element methods for the mixed Navier–Stokes/Darcy model. *Int. J. Comput. Math.* 93 (7), 1155–1172.
- Cai, M., Mu, M., Xu, J., 2009. Numerical solution to a mixed Navier–Stokes/Darcy model by the two-grid approach. *SIAM J. Numer. Anal.* 47 (5), 3325–3338.
- Chidyagwai, P., Rivière, B., 2010. Numerical modelling of coupled surface and subsurface flow systems. *Adv. Water Res.* 33 (1), 92–105.
- Blackford, Blackford, Jerry, Alendal, Guttorm, Artioli, Yuri, Avlesen, Helge, Cazenave, Pierre, Chen, Baixin, Dale, Andy, Dewar, Marius, García, Ibáñez, Maribel, I., Gros, Jonas, Gundersen, Kristian, Haeckel, Matthias, Khajepor, Sorush, Lessin, Gennadi, Oleyunik, Anna, Omar, Abdurahman M., Saleem, Umer, et al., 2018. Ensuring efficient and robust offshore storage – the role of marine system modelling. In: 14th Greenhouse Gas Control Technologies Conference Melbourne 21–26 October, 2018 (GHGT-14). Available at SSRN. <https://ssrn.com/abstract=3365821>.
- Taylor, P., et al., 2015. A novel sub-seabed CO₂ release experiment informing monitoring and impact assessment for geological carbon storage. *Int. J. Greenhouse Gas Control* 38, 3–17.
- Dean, M., Tucker, O., 2017. A risk-based framework for Measurement, Monitoring and Verification (MMV) of the Goldeneye storage complex for the Peterhead CCS project, UK. *Int. J. Greenhouse Gas Control* 61, 1–15.
- Floh, A., et al., 2020. Towards improved monitoring of offshore carbon storage: A real-world field experiment detecting a controlled sub-seafloor CO₂ release, no. This Issue. *Int. J. Greenhouse Gas Control*.
- Floh, A., et al., 2021. Towards improved monitoring of offshore carbon storage: a real-world field experiment detecting a controlled sub-seafloor CO₂ release. *Int. J. Greenhouse Gas Control* 106, 103237.
- Lichtschlag, A., et al., 2021. Impact of CO₂ leakage from sub-seabed carbon dioxide storage on sediment and porewater geochemistry. *Int. J. Greenhouse Gas Control* (STEMM-CCS).
- Phillips, E., Merritt, J., 2008. Evidence for multiphase water-escape during rafting of shelly marine sediments at Clava, Inverness-shire, NE Scotland. *Quat. Sci. Rev.* 27 (9), 988–1011.
- Henderson, N., Brétas, J., Sacco, W., 2010. A three-parameter Kozeny–Carman generalized equation for fractal porous media. *Chem. Eng. Sci.* 65, 4432–4442.
- openfoam.org. (n.d.). 2020 OpenFOAM | Free CFD Software | The OpenFOAM Foundation. [online] Available at: <https://openfoam.org/>.
- Radwan, A.E., et al., 2019. Pore and fracture pressure modeling using direct and indirect methods in Badri Field, Gulf of Suez, Egypt. *J. Afr. Earth Sci.* 156, 133–143.
- Gor, G.Y., Stone, H.A., Prévost, J.H., 2013. Fracture propagation driven by fluid outflow from a low-permeability aquifer. *Transp. Porous Media* 100, 69–82.
- Rusche, H., 2002. Computational Fluid Dynamics of Dispersed Two-Phase Flows at High Phase Fractions, in Department of Mechanical Engineering, University of London and Diploma of Imperial College.
- Darcy, H.P.G., 1856. *Les Fontaines Publiques de la Ville de Dijon*. Victor Dalmont, Paris.
- Brooks, R.H.a.C., A. T., Hydraulic properties of porous media. *Hydrology Papers*, No. 3, Colorado State U., Fort Collins, Colorado. 1964.
- Corey, A.T., 1954. The interrelation between gas and oil relative permeabilities. *Interrelation between Gas Oil Relat. Permeabilities* 38–41.
- Jiang, L., et al., 2017. Mass transfer coefficient measurement during brine flush in a CO₂-filled packed bed by X-ray CT scanning. *Int. J. Heat Mass Transfer* 115, 615–624.
- Jiang, L., et al., 2018. Displacement and dissolution characteristics of CO₂/brine system in unconsolidated porous media. *Transp. Porous Media* 122 (3), 595–609.
- Duan, J., et al., 2015. Hydro dynamic modeling of stratified smooth two-phase turbulent flow with curved interface through circular pipe. *Int. J. Heat Mass Transfer* 89, 1034–1043.
- Chisholm, D., 1980. Two-phase flow in bends. *Int. J. Multiphase Flow* 6 (4), 363–367.
- Koopmans, D., et al., 2021. Detection and quantification of carbon dioxide gas at the seafloor using pH eddy covariance and measurements of plume advection. *Int. J. Greenhouse Gas Control* (STEMM-CCS).